The synchrotron self-Compton spectrum of relativistic blast waves at large Y

Martin Lemoine[★]

Institut d'Astrophysique de Paris, CNRS, UPMC, 98 bis boulevard Arago, F-75014 Paris, France

ABSTRACT

Recent analyses of multiwavelength light curves of gamma-ray bursts afterglows point to values of the magnetic turbulence well below the canonical ∼1 per cent of equipartition, in agreement with theoretical expectations of a microturbulence generated in the shock precursor, which then decays downstream of the shock front through collisionless damping. As a direct consequence, the Compton parameter Y can take large values in the blast. In the presence of decaying microturbulence and/or as a result of the Klein–Nishina suppression of inverse Compton cooling, the Y parameter carries a non-trivial dependence on the electron Lorentz factor, which modifies the spectral shape of the synchrotron and inverse Compton components. This paper provides detailed calculations of this synchrotron self-Compton spectrum in this large Y regime, accounting for the possibility of decaying microturbulence. It calculates the expected temporal and spectral indices α and β customarily defined by $F_\nu \propto t_{\rm obs}^{-\alpha} \nu^{-\beta}$ in various spectral domains. This paper also makes predictions for the very high energy photon flux; in particular, it shows that the large Y regime would imply a detection rate of gamma-ray bursts at $>10\,{\rm GeV}$ several times larger than currently anticipated.

Key words: acceleration of particles – shock waves – gamma-ray burst: general.

1 INTRODUCTION

The afterglow radiation of gamma-ray bursts (GRBs), which spans the range from the radio domain to the X-ray and possible higher frequencies, with a characteristic decrease in time of the peak flux, is nicely interpreted in terms of the synchrotron radiation of ultrarelativistic electrons that have been accelerated at the forward ultrarelativistic collisionless shock wave of the outflow, see e.g. Piran (2004) for a detailed review.

This model thus opens a beautiful connection between astronomical data and the microphysics of the rather extreme phenomena that relativistic collisionless shocks represent. Zooming in on microphysical scales reveals the shock front as a microturbulent magnetic barrier which isotropizes the incoming background plasma, see e.g. Moiseev & Sagdeev (1963) for pioneering studies, and Kato & Takabe (2008) and Spitkovsky (2008a) for detailed numerical simulations. This microturbulent barrier itself results from the build-up of electromagnetic microinstabilities ahead of the shock front, in the shock precursor where suprathermal particles mix with the incoming background plasma, e.g. Medvedev & Loeb (1999), Wiersma & Achterberg (2004), Lyubarsky & Eichler (2006), Achterberg & Wiersma (2007), Achterberg, Wiersma & Norman (2007), Bret, Gremillet & Bénisti (2010), Lemoine & Pelletier (2010, 2011),

Rabinak, Katz & Waxman (2011), Shaisultanov, Lyubarsky & Eichler (2012) and Lemoine et al. (2014a,b).

The resulting microturbulence, with typical length-scale $\lambda_{\delta B} \sim c/\omega_{\rm pi}$ ($\omega_{\rm pi}$ the ion plasma frequency) and typical strength[1] $\epsilon_B \sim 0.01$, thus emerges as a key ingredient for the microphysics of collisionless shocks. Actually, it also represents a key requisite for the relativistic Fermi process, since this latter can take place (in ideal conditions) only when an intense microturbulence, with power on scales smaller than the gyroradius of the accelerated particles, is able to unlock the particles off the background magnetic field lines, by scattering them faster than a gyration time in this background field (Lemoine, Pelletier & Revenu 2006; Niemiec, Ostrowski & Pohl 2006; Pelletier, Lemoine & Marcowith 2009). In terms of magnetization $\sigma = B^2/\left(8\pi 4\Gamma_{\rm b}^2 nm_{\rm p}c^2\right)$, with B the background field expressed in the downstream frame, this condition amounts to $\sigma \ll \epsilon_B^2$ (Lemoine & Pelletier 2010, 2011; Lemoine et al. 2014a), a condition which is indeed satisfied for the forward shock of GRBs, since $\sigma \sim 10^{-9}$ in the interstellar medium. This point of view has been confirmed by particle-in-cell (PIC) simulations (e.g. Spitkovsky 2008b, Martins et al. 2009; Nishikawa et al.

---

[1] $\epsilon_B \equiv \delta B^2/\left(8\pi 4\Gamma_{\rm b}^2 nm_{\rm p}c^2\right)$ represents the magnetic energy fraction of equipartition, if $\Gamma_{\rm b} \gg 1$ represents the relative Lorentz factor between upstream and downstream, and n the upstream proper density.

★E-mail: lemoine@iap.fr

2009; Sironi & Spitkovsky 2009, 2011; Haugbølle 2011; Sironi, Spitkovsky & Arons 2013).

Finally, these microinstabilities may also build the magnetized turbulence in which the electrons eventually produce the afterglow radiation in a synchrotron-like process (Medvedev & Loeb 1999) – jitter effects are expected to be weak in the conditions typical of those shock waves – provided it survives collisonless damping downstream of the shock front (Gruzinov & Waxman 1999). Recent analyses of the damping of this Weibel-type microturbulence yield a damping rate $\propto k^3$, where k denotes a turbulent wavenumber, indicating that small scales are dissipated first, but that large scales may survive longer (Chang, Spitkovsky & Arons 2008; Lemoine 2015). In turn, this implies that the turbulence strength, or ϵ_B, should decay as a power law in (proper) time (or distance) downstream of the shock front, with an index which itself depends on the (unknown) microturbulent power spectrum at the shock front. Interestingly, this time dependence of ϵ_B turns out to be encoded in the multiwavelength synchrotron spectrum, since electrons of different Lorentz factors cool at different times, hence in regions of different magnetic field strengths (Rossi & Rees 2003; Derishev 2007; Lemoine 2013).

Although one cannot exclude that other external instabilities would pollute the blast with magnetized turbulence, it is tempting to consider that the generation of microturbulence could be responsible at the same time for the formation of the shock, for the acceleration of particles and for the radiation of these particles. It is furthermore tempting to follow this thread to use the multiwavelength spectrum of GRBs as a tomograph of the magnetized turbulence. As a matter of fact, the recent detections of extended emission of GRBs in the >100 MeV band by the *Fermi*-LAT instrument do point to a net decay of the microturbulence behind the shock front (Lemoine, Li & Wang 2013), with $\epsilon_B \propto (t\omega_{\rm pi}/100)^{\alpha_t}$ and $-0.5 \lesssim \alpha_t \lesssim -0.4$. This argument can be recapped as follows: if the accelerated particles scatter in a microturbulence, the maximal synchrotron photon energy is limited to a few GeV at an observer time of 100 s (Kirk & Reville 2010; Plotnikov, Pelletier & Lemoine 2013; Sironi et al. 2013; Wang, Liu & Lemoine 2013); this maximal energy scales as the square root of ϵ_{B+}, i.e. the magnitude of the turbulence in the vicinity of the shock front, and the above value assumes $\epsilon_{B+} = 0.01$. Therefore, the interpretation of this extended >100 MeV emission as a synchrotron process points to the existence of a strong microturbulence close to the shock front; on the other hand, multiwavelength fits of the afterglows for these *Fermi*-LAT GRBs indicate that low-energy photons are produced in regions of rather low ϵ_{B-}, of the order of 10^{-6}–10^{-5}. This discrepancy between ϵ_{B-} and ϵ_{B+} is naturally interpreted as the decay of the microturbulence through collisionless damping. As discussed in Lemoine et al. (2013), the decay rate $\alpha_t \sim -0.5$ to -0.4 further matches the results of a detailed numerical experiment reported in Keshet et al. (2009).

The decay of microturbulence has also been proposed as a possible solution to the abnormal spectral indices observed in the prompt emission phase (Derishev 2007), but admittedly, the physics of mildly relativistic shock waves may well differ from that of ultrarelativistic shock waves; in particular, the extended precursor size in mildly relativistic shocks opens the way to other instabilities operating on larger length-scales. Although the present considerations can also be generalized to the case of internal shocks, all of the discussion that follows will focus on the external ultrarelativistic shock front.

An interesting consequence of a decaying microturbulence, or more generally, of a low average value of ϵ_B as measured in

the *Fermi*-LAT and other bursts (e.g. Kumar & Barniol-Duran 2009, 2010; He et al. 2011; Barniol-Duran 2014; Santana, Barniol-Duran & Kumar 2014), is a large Compton parameter Y, at least if one omits the influence of Klein–Nishina (KN) effects, which actually depend on electron energy and hence on observed frequency, see below. Recall indeed that in the standard model, assuming that electrons cool through inverse Compton (IC) interactions on their synchrotron spectrum in the Thomson limit (i.e. neglecting KN effects), $Y \sim (\eta \epsilon_e / \epsilon_B)^{1/2}$ at $Y \gg 1$, with $\eta \simeq \min[1, (\gamma_c/\gamma_m)^{2-p}]$ the cooling efficiency of electrons, γ_c denoting the Lorentz factor of electrons which cool on a dynamical time-scale, γ_m the minimum Lorentz factor of the injected electron power law and $-p$ the index of this power law, e.g. Panaitescu & Kumar (2000), Sari & Esin (2001) and Piran (2004). This Y parameter also reflects the power of the IC component relatively to the synchrotron component, and therefore the ratio of emission at very high energies to that in the X-ray range. The possibility of a large Y parameter should thus increase the chances of observing GRBs at very high energies with upcoming Čerenkov telescopes. The observation of this IC component would then open a new spectral domain with which one could study the microphysics of the turbulence in the blast.

However, the computation of the synchrotron self-Compton (SSC) spectrum of the blast in the large Y regime is not trivial because the shape of the synchrotron spectrum influences the cooling history of the electrons, which itself determines the synchrotron spectral shape. In particular, the KN suppression of the IC cross-section may itself modify this cooling history, and hence modify the very shape of the synchrotron spectrum, see Nakar, Ando & Sari (2009) and Wang et al. (2010); see also Barniol-Duran & Kumar (2011) for the particular case of GRB090902B and Bošnjak, Daigne & Dubus (2009) and Daigne, Bošnjak & Dubus (2011) for related discussions in the context of GRB prompt emission. In the case of decaying microturbulence, this issue is more acute, because the synchrotron power νF_ν may be rising with frequency, due to the fact that lower frequency photons are emitted by electrons of longer cooling time, in regions of lower magnetic field strength (Lemoine 2013). Therefore, the Lorentz factor-dependent KN limit determines the radiation intensity on which an electron can cool. Finally, so far the influence of decaying microturbulence on the synchrotron spectrum has been studied for a fixed Y parameter, independent of electron Lorentz factor; hence, the general shape of the SSC spectrum is not known in this physically relevant case.

These considerations motivate the present study, which calculates the SSC spectrum for a relativistic blast wave in the large Y regime. Although the prime objective is to understand how the decaying microturbulence affects the SSC spectrum, the present discussion also addresses the case of a uniform, low value of ϵ_B. The results are applied to the case of the GRB afterglows, by calculating the spectrum at various observer times and by plotting, in particular, the spectral slopes in various frequency windows. The spectrum is also evaluated in the multi-GeV range, with a proper account of synchrotron and SSC contributions, to make clear predictions for future Čerenkov observatories such as HAWK and CTA.

This paper is organized as follows: Section 2 presents an analytical description of the spectrum in the slow-cooling limit, accounting for KN effects, and introduces a fast algorithm to compute this spectrum in the fast-cooling regime; Section 3 then computes the light curves and plots the temporal and spectral indices α and β, commonly defined by $F_\nu \propto t_{\rm obs}^{-\alpha} \nu^{-\beta}$, and gives predictions for the very high energy photon flux; finally, Section 4 summarizes these results and provides some conclusions.

2 SSC SPECTRUM

2.1 Set-up

The set-up is as follows: electrons are swept up by a relativistic shock front propagating in a density profile $n \propto r^{-k}$, then accelerated on a short time-scale to a power law $dN_{e,0}/d\gamma \propto \gamma^{-p}\Theta(\gamma - \gamma_m)$ above a minimal Lorentz factor γ_m. The minimal Lorentz factor is defined as usual by $\gamma_m \equiv \epsilon_e \Gamma_b m_p/m_e(p - 2)/(p - 1)$, with $\epsilon_e \sim 0.1$. Cooling takes place on much longer time-scales. When describing the cooling history, the total IC cross-section is modelled as a top-hat, with $\sigma = \sigma_T$ for $\nu < \tilde{\nu}(\gamma)$ and zero otherwise, and $\tilde{\nu}(\gamma)$ denoting the frequency of photons with which electrons of Lorentz factor γ interact at the KN limit (Nakar et al. 2009; Wang et al. 2010), i.e.

$$\tilde{\nu} \equiv \frac{\Gamma_b m_e c^2}{h\gamma(1 + z)}. \tag{1}$$

All frequencies are written in the observer rest frame; as mentioned above, Γ_b denotes the Lorentz factor of the blast in the source rest frame. The Compton parameter can then be approximated as

$$Y(\gamma) \simeq \frac{U_{\mathrm{rad}}[\nu < \tilde{\nu}(\gamma)]}{U_B(\gamma)}, \tag{2}$$

where

$$U_{\mathrm{rad}}[< \tilde{\nu}(\gamma)] = \int_0^{\tilde{\nu}(\gamma)} d\nu \, U_\nu(\nu) \tag{3}$$

represents the comoving radiation energy density at frequencies $\nu < \tilde{\nu}(\gamma)$, on which the electron of Lorentz factor γ can cool. Of course, if $\tilde{\nu} > \nu_{\mathrm{peak}}$ at which the differential energy density $U_\nu(\nu)$ reaches its maximum, then $U_{\mathrm{rad}}[\nu < \tilde{\nu}(\gamma)] \sim \nu_{\mathrm{peak}}U_{\nu_{\mathrm{peak}}} \sim U_{\mathrm{rad}}$ and it does not depend on γ (U_{rad} denotes here the total comoving energy density). In principle, U_{rad} includes all forms of radiation, synchrotron and IC alike; however, multiple Compton scattering can be neglected for standard GRB parameters, and hence U_{rad} is hereafter determined with the synchrotron spectrum only.

The quantity $U_B(\gamma)$ represents the energy density contained in the magnetic field and it depends on γ if the turbulence decays in (proper) time behind the shock, because electrons of different Lorentz factors then cool in regions of different magnetic field strengths. In this work, the decay law of the turbulence takes the power-law form $\epsilon_B(t) \propto t^{\alpha_t}$ far from the shock front and $\epsilon_B \sim \epsilon_{B+} = 0.01$ close to the shock front. How far is expressed in terms of the proper time t since the plasma element was injected through the shock, i.e. $t \equiv x/\beta_d$ in terms of the downstream (comoving) distance to the shock front x and β_d, the shock front velocity relative to the downstream rest frame. According to PIC simulations, the characteristic (temporal) scale Δ separating far from close to the shock front is $\Delta \sim 10^{2-3} \omega_{\mathrm{pi}}$, see Chang et al. (2008) and Keshet et al. (2009) for simulations, as well as Lemoine (2013, 2015) for discussions of this issue; for reference, $\omega_{\mathrm{pi}}^{-1} \sim 7.5 \times 10^{-4} n_0^{-1/2}$ s for a relativistic blast wave propagating in a medium of proton density n_0 cm^{-3}. The uncertainty on the value of Δ does not really influence the results presented below, because it can be embedded in that associated with the decay power-law exponent α_t. Recent work mentioned above suggests $\alpha_t \sim -0.5 \rightarrow -0.4$ for a decay law $\epsilon_B \sim \epsilon_{B+}(t\omega_{\mathrm{pi}}/100)^{\alpha_t}$; hence, the following adopts $\Delta = 100\omega_{\mathrm{pi}}^{-1}$ and $\alpha_t = -0.4$. This decay implies that the minimum magnetic field in the blast, close to the contact discontinuity, is characterized by the equipartition fraction $\epsilon_{B-} = \epsilon_{B+}(t_{\mathrm{dyn}}/\Delta)^{\alpha_t}$ in terms of the dynamical time-scale $t_{\mathrm{dyn}} = r/(\Gamma_b c)$. Typical values are $t_{\mathrm{dyn}} \sim 10^5-10^6$ s at an observer time of 10^4 s (e.g. $\Gamma_b \sim 20-30$ and $r \sim 10^{17}-$

10^{18} cm), with a mild dependence on the model parameters, leading to values of the order of $\epsilon_{B-} \sim 10^{-5}$ for $\alpha_t \sim -0.5$. Note that $t_{\mathrm{dyn}}/\Delta \propto t_{\mathrm{obs}}^{(5-2k)/(8-2k)}$ evolves slowly as a function of observer time, and hence so does ϵ_{B-}.

In this work, it is assumed that a particle emits its synchrotron radiation at the location at which it cools, if it cools on a dynamical time-scale; in the opposite limit, it is assumed that it emits its synchrotron photons in the magnetic field close to the contact discontinuity, of strength δB_- (associated with the parameter ϵ_{B-}). The justification of this approximation is as follows: the energy emitted in synchrotron photons by a particle up to time t, along its trajectory downstream of the shock, can be written as

$$E_{\mathrm{syn}} = \frac{1}{6\pi}\sigma_T c \int_0^t d\tau \, \delta B^2(\tau)\gamma_e^2(\tau)\beta_e^2(\tau) \tag{4}$$

as a function of the time-dependent Lorentz factor $\gamma_e(\tau)$ of the particle along its cooling trajectory, with $\beta_e(\tau) \sim 1$ the particle velocity in units of c. One can then show that E_{syn} is dominated by the contribution at $t \sim t_{\mathrm{cool}}(\gamma)$, where γ denotes the initial value $\gamma_e(0)$, as follows. At early times $\tau \ll t_{\mathrm{cool}}(\gamma)$, $\gamma_e(\tau) \sim \gamma$ and the integrand scales as $U_B(\tau) \propto \tau^{\alpha_t}$; hence, the integral is dominated by the large time behaviour if $\alpha_t > -1$, which is indeed an explicit assumption of the present work. At late times $\tau \gg t_{\mathrm{cool}}(\gamma)$, one can obtain an upper bound on how fast $\gamma_e(\tau)$ decreases by considering synchrotron losses only, i.e. by neglecting IC losses. The integration of

$$\frac{d\gamma_e}{d\tau} = -\frac{4}{3}\frac{\sigma_T c U_B(\tau)}{m_e c^2}\gamma_e^2(\tau)\beta_e(\tau)^2 \tag{5}$$

leads to $\gamma_e(\tau) \sim \gamma \, [\tau/t_{\mathrm{cool}}(\gamma)]^{-1-\alpha_t}$ for $\tau \gg t_{\mathrm{cool}}(\gamma)$. Therefore, the integrand in equation (4) behaves as $\tau^{-2-\alpha_t}$ for $\tau > t_{\mathrm{cool}}(\gamma)$; hence, E_{syn} is indeed dominated by the contribution at $t \sim t_{\mathrm{cool}}(\gamma)$ provided $\alpha_t > -1$.

This thus supports the above approximation that a particle with initial Lorentz factor $\gamma > \gamma_c$ emits its synchrotron radiation on a magnetic field of strength $\delta B[t_{\mathrm{cool}}(\gamma)]$, with $t_{\mathrm{cool}}(\gamma)$ the cooling time of the particle. Of course, if $t_{\mathrm{cool}}(\gamma) > t_{\mathrm{dyn}}$, the particle does not actually cool, and E_{syn} is then dominated by the upper bound $t \sim t_{\mathrm{dyn}}$, i.e. particles radiate synchrotron radiation in the relaxed magnetic field at the back of the blast, of strength δB_-.

Since $t_{\mathrm{cool}}(\gamma_c) = t_{\mathrm{dyn}}$ by definition, and since $\delta B(t_{\mathrm{dyn}}) = \delta B_-$, also by definition,

$$U_B(\gamma) \simeq U_{B-}\max\left[1, \left(\frac{t_{\mathrm{cool}}(\gamma)}{t_{\mathrm{dyn}}}\right)^{\alpha_t}\right] \tag{6}$$

with $U_{B-} \equiv \delta B_-^2/(8\pi) = U_B(\gamma_c)$.

In line with the above discussion, electrons of Lorentz factor γ radiate their energy through synchrotron at a typical frequency

$$\nu_{\mathrm{syn}}(\gamma) \propto \delta B[t_{\mathrm{cool}}(\gamma)]\gamma^2 \simeq \nu_c \left[\frac{t_{\mathrm{cool}}(\gamma)}{t_{\mathrm{dyn}}}\right]^{\alpha_t/2}\left(\frac{\gamma}{\gamma_c}\right)^2. \tag{7}$$

Here, $\nu_c \equiv \nu_{\mathrm{syn}}(\gamma_c)$ denotes the synchrotron peak frequency for particles of Lorentz factor γ_c.

Finally, the cooling time-scale can be written as

$$t_{\mathrm{cool}}(\gamma) \simeq t_{\mathrm{dyn}} \frac{1 + Y_c}{1 + Y(\gamma)}\frac{U_{B-}}{U_B(\gamma)}\frac{\gamma_c}{\gamma},$$

$$\simeq t_{\mathrm{dyn}}\left[\frac{1 + Y(\gamma)}{1 + Y_c}\right]^{-1/(1+\alpha_t)}\left(\frac{\gamma}{\gamma_c}\right)^{-1/(1+\alpha_t)}. \tag{8}$$

The second equality is obtained by replacing $U_B(\gamma)/U_{B-}$ with its value given in equation (6), assuming $\gamma > \gamma_c$.

Equations (2), (6), (7) and (8) then allow one to derive the following scalings for $\gamma > \gamma_c$:

$$\frac{U_B(\gamma)}{U_{B-}} \simeq \left[\frac{1 + Y(\gamma)}{1 + Y_c}\right]^{-\alpha_t/(1+\alpha_t)} \left(\frac{\gamma}{\gamma_c}\right)^{-\alpha_t/(1+\alpha_t)}, \qquad (9)$$

$$\frac{\nu_{\mathrm{syn}}(\gamma)}{\nu_c} \simeq \left[\frac{1 + Y(\gamma)}{1 + Y_c}\right]^{-\alpha_t/[2(1+\alpha_t)]} \left(\frac{\gamma}{\gamma_c}\right)^{2-\alpha_t/[2(1+\alpha_t)]}, \qquad (10)$$

$$\frac{Y(\gamma)\,[1 + Y(\gamma)]^{-\alpha_t/(1+\alpha_t)}}{Y_c(1 + Y_c)^{-\alpha_t/(1+\alpha_t)}} \simeq \frac{U_{\mathrm{rad}}(\nu < \tilde{\nu})}{U_{\mathrm{rad}}(\nu < \tilde{\nu}_c)} \left(\frac{\gamma}{\gamma_c}\right)^{\alpha_t/[(1+\alpha_t)]}. \qquad (11)$$

Y_c stands for $Y(\gamma_c)$.

Once the ratio $U_{\mathrm{rad}}(\nu < \tilde{\nu})/U_{\mathrm{rad}}(\nu < \tilde{\nu}_c)$ – which captures KN effects – has been specified, it is possible to derive the scalings of $Y(\gamma)$ as a function of γ, and hence of $\nu_{\mathrm{syn}}(\gamma)$. One should emphasize that in the above expressions, γ represents the initial Lorentz factor of the particle, after acceleration has shaped the power law, but before cooling has effectively taken place.

2.2 Synchrotron spectrum

Standard calculations of the synchrotron spectrum of a blast wave generally derive the stationary electron distribution in the blast, by solving a transport equation in momentum space, averaged over the depth of the blast, accounting for injection of the power law at the shock and for cooling downstream (e.g. Sari, Piran & Narayan 1998; Sari & Esin 2001); this yields a standard broken power-law shape $\mathrm{d}N_e/\mathrm{d}\gamma_e$ with indices -2 for $\gamma_c < \gamma < \gamma_m$ or $-p$ for $\gamma_m < \gamma < \gamma_c$ and $-p - 1$ for $\max(\gamma_c, \gamma_m) < \gamma$. However, one can also derive the synchrotron spectrum by a direct mapping of the energy initially stored into the electron population to that radiated in synchrotron; this approach is simpler in the present case and it works as follows.

Electrons injected with Lorentz factor $\gamma > \max(\gamma_m, \gamma_c)$ emit a fraction $[1 + Y(\gamma)]^{-1}$ of their energy in synchrotron radiation; the energy density contained in such electrons (within an interval $\mathrm{d}\ln\gamma$) is itself a fraction $(p - 2)(\gamma/\gamma_m)^{2-p}\,\mathrm{d}\ln\gamma$ of the energy density U_e contained in electrons immediately behind the shock front, before cooling has started to take place; $U_e = \epsilon_e\,4\Gamma_b^2 n m_p c^2$. Consequently, the synchrotron flux received at frequency $\nu = \nu_{\mathrm{syn}}(\gamma)$ can be written as

$$\nu F_{\nu,\mathrm{syn}} \simeq \frac{1}{4\pi D_L^2} \frac{4}{3} \Gamma_b^2 \frac{4\pi r^2 c(p-2)U_e}{1 + Y(\gamma)} \left(\frac{\gamma}{\gamma_m}\right)^{2-p} \frac{\mathrm{d}\ln\gamma}{\mathrm{d}\ln\nu}. \qquad (12)$$

The above assumes $p > 2$, but it can be generalized to any index $p > 1$. Indeed, the above picture assumes that particles with $\gamma > \max(\gamma_m, \gamma_c)$ radiate their energy at $\nu_{\mathrm{syn}}(\gamma)$ and then do not contribute anymore to the synchrotron spectrum, which is a reasonable approximation if $p > 1$; if $p < 1$, in contrast, the radiation of the high-energy particles during their complete cooling history dominates that of the lower energy ones.

Similarly, one can write down the flux for $\gamma_m > \gamma > \gamma_c$ or $\gamma_c > \gamma > \gamma_m$, whichever occurs, as follows:

$$\nu F_{\nu,\mathrm{syn}} \simeq \nu_m F_{\nu_m,\mathrm{syn}} \begin{cases} \dfrac{\gamma}{\gamma_m} \dfrac{1 + Y_m}{1 + Y} & (\gamma_m > \gamma > \gamma_c) \\[2ex] \left(\dfrac{\nu}{\nu_m}\right)^{(3-p)/2} & (\gamma_c > \gamma > \gamma_m) \end{cases} \qquad (13)$$

with $Y_m \equiv Y(\gamma_m)$ and $\nu_m = \nu_{\mathrm{syn}}(\gamma_m)$. The spectrum at $\nu < \nu_c$ is indeed unchanged with respect to the standard case, although the value of U_{B-} must be used to compute the characteristic frequencies. Regarding the fast-cooling limit $\gamma_c < \gamma < \gamma_m$, the factor can be understood by noting that all injected particles with $\gamma > \gamma_m$ shift from γ to γ_c during their cooling history, and that at each point along this cooling trajectory they radiate (in synchrotron) a fraction $(\gamma/\gamma_m)(1 + Y_m)/(1 + Y)$ of the energy radiated (in synchrotron) by a particle of Lorentz factor γ_m. Note also that in the limits $\alpha_t \to 0$, $Y(\gamma) \ll 1$, one recovers the usual scaling $\nu F_{\nu,\mathrm{syn}} \propto \nu^{1/2}$ since $\nu \propto \gamma^2$.

Provided γ_c and Y_c are given, one can derive $\nu_{\mathrm{syn}}(\gamma)$ and $Y(\gamma)$, and hence $\gamma(\nu)$ and $Y(\nu)$ by using equations (9)–(11), and then $\nu F_{\nu,\mathrm{syn}}$ using equations (12) and (13). Consider as an example the case $Y \gg 1$, omitting KN effects, i.e. $\tilde{\nu} \to +\infty$ for all ν: for $\gamma > \gamma_c$, one derives $Y(\gamma) \propto \gamma^{\alpha_t}$ from equation (11), $\nu_p \propto \gamma^{2-\alpha_t/2}$ from equation (10) and $\nu F_{\nu,\mathrm{syn}} \propto \gamma^{2-p}/(1 + Y) \propto \nu^{(2-p-\alpha_t)/(2-\alpha_t/2)}$ from equation (12). This latter scaling matches the explicit calculation of Lemoine (2013), which computes the integrated cooling history of the electron power law in the decaying magnetic field. This example also confirms that $\nu F_{\nu,\mathrm{syn}}$ rises with ν if $\alpha_t \lesssim 2 - p$; hence, KN effects should not be omitted in an accurate calculation of $\nu F_{\nu,\mathrm{syn}}$.

The above provides the tools needed to calculate the synchrotron spectrum; explicit calculations in both the slow- and the fast-cooling regimes are provided in the following sections.

2.3 IC spectrum

In order to calculate the IC emissivity, the synchrotron spectral density $F_{\nu,\mathrm{syn}}$ must be folded over the Compton cross-section and the cooled particle distribution, integrated over the blast. The following derivation of the cooled distribution function relies on the observations that $\mathrm{d}t_{\mathrm{cool}}(\gamma)/\mathrm{d}\gamma < 0$ and that the cooling history $\gamma_{\mathrm{cool}}(t)$ at times $t > t_0$ does not depend on the history at times $t < t_0$, i.e. electrons of various Lorentz factor follow a universal cooling trajectory $\gamma_{\mathrm{cool}}(t)$.

One writes $\mathrm{d}\dot{N}_{e,0}$ the (comoving) rate at which electrons are swept up and accelerated into a power law in a Lorentz factor interval $\mathrm{d}\gamma$. One also defines $\mathrm{d}N_e$, which represents the total number of electrons in the blast in a Lorentz factor interval $\mathrm{d}\gamma_e$; note the difference of notation: γ_e refers to a value of the Lorentz factor of the blast-averaged distribution, while γ corresponds to the Lorentz factor of the injection distribution, i.e. before cooling has occurred.

The injection of particles with Lorentz factor γ populates the downstream with particles of Lorentz factor $\gamma_e = \gamma$ over a fraction $t_{\mathrm{cool}}/t_{\mathrm{dyn}}$ of the depth of the blast. In contrast, particles injected with $\gamma_c > \gamma > \gamma_m$ retain their Lorentz factor (no cooling) and populate the whole blast. Therefore, one can write the average distribution for $\gamma_e > \gamma_m$ as

$$\frac{\mathrm{d}N_e}{\mathrm{d}\gamma_e} \simeq \frac{\mathrm{d}\dot{N}_{e,0}}{\mathrm{d}\gamma}(\gamma = \gamma_e) \min\left[t_{\mathrm{dyn}}, t_{\mathrm{cool}}(\gamma)\right] \quad (\gamma > \gamma_m). \qquad (14)$$

Note also that t_{dyn} sets the scale for adiabatic losses, while t_{cool} sets the scale for radiative losses.

In the fast-cooling regime, all electrons injected with Lorentz factor $\gamma > \gamma_m$ cool down to γ_c, following the same cooling history $\gamma_{\mathrm{cool}}(\tau)$; therefore,

$$\frac{\mathrm{d}N_e}{\mathrm{d}\gamma_e} \simeq \int_0^{t_{\mathrm{dyn}}} \mathrm{d}\tau \int_{\gamma_m}^{+\infty} \mathrm{d}\gamma \frac{\mathrm{d}\dot{N}_{e,0}}{\mathrm{d}\gamma} \delta\left[\gamma_e - \gamma_{\mathrm{cool}}(\tau)\right]$$

$$\simeq \dot{N}_{e,0} \frac{t_{\mathrm{cool}}(\gamma_e)}{\gamma_e}, \qquad (15)$$

where $\dot{N}_{\rm e,0} = \int_{\gamma_{\rm m}}^{+\infty} {\rm d}\gamma \, {\rm d}\dot{N}_{\rm e,0}/{\rm d}\gamma$ represents the total injection rate of electrons. The last expression in equation (15) follows from the definition $t_{\rm cool}(\gamma_{\rm e}) = \gamma_{\rm e}|{\rm d}\gamma_{\rm e}/{\rm d}t|^{-1}$ after interchanging the integrals.

Using the scaling of $t_{\rm cool}(\gamma)$, one then derives

$$\frac{{\rm d}N_{\rm e}}{{\rm d}\gamma_{\rm e}} \simeq \frac{\dot{N}_{\rm e,0} t_{\rm dyn}}{\gamma_{\rm m}} \left(\frac{\gamma_{\rm e}}{\gamma_{\rm m}}\right)^{-p} \qquad (\gamma_{\rm m} < \gamma_{\rm e} < \gamma_{\rm c})$$

$$\frac{{\rm d}N_{\rm e}}{{\rm d}\gamma_{\rm e}} \simeq \frac{\dot{N}_{\rm e,0} t_{\rm dyn}}{\gamma_{\rm m}} \left(\frac{\gamma_{\rm e}}{\gamma_{\rm m}}\right)^{-1} \left(\frac{\gamma_{\rm e}}{\gamma_{\rm c}}\right)^{-1/(1+\alpha_t)}$$
$$\times \left[\frac{1 + Y(\gamma_{\rm e})}{1 + Y_{\rm c}}\right]^{-1/(1+\alpha_t)} \qquad (\gamma_{\rm c} < \gamma_{\rm e} < \gamma_{\rm m})$$

$$\frac{{\rm d}N_{\rm e}}{{\rm d}\gamma_{\rm e}} \simeq \frac{\dot{N}_{\rm e,0} t_{\rm dyn}}{\gamma_{\rm m}} \left(\frac{\gamma_{\rm e}}{\gamma_{\rm m}}\right)^{-p} \left(\frac{\gamma_{\rm e}}{\gamma_{\rm c}}\right)^{-1/(1+\alpha_t)}$$
$$\times \left[\frac{1 + Y(\gamma_{\rm e})}{1 + Y_{\rm c}}\right]^{-1/(1+\alpha_t)} \qquad [\max(\gamma_{\rm c}, \gamma_{\rm m}) < \gamma_{\rm e}].$$
$$(16)$$

In the limit $\alpha_t \to 0$, one recovers ${\rm d}N_{\rm e}/{\rm d}\gamma_{\rm e} \propto [1 + Y(\gamma_{\rm e})]^{-1} \gamma_{\rm e}^{-2}$ for $\gamma_{\rm c} < \gamma_{\rm e} < \gamma_{\rm m}$ or ${\rm d}N_{\rm e}/{\rm d}\gamma_{\rm e} \propto [1 + Y(\gamma_{\rm e})]^{-1}\gamma^{-p-1}$ for $\gamma_{\rm m} < \gamma_{\rm c} < \gamma_{\rm e}$; both match the expressions derived in Nakar et al. (2009) and in Wang et al. (2010) for a homogeneous (non-decaying) turbulence.

It is also instructive to show that the above average electron distribution, when associated with the appropriate (i.e. Lorentz factor-dependent) magnetic field, leads to the same scalings for the synchrotron spectrum as equations (12) and (13). Consider for instance the regime $\gamma > \max(\gamma_{\rm c}, \gamma_{\rm m})$: the average synchrotron power of the blast scales as $\nu F_{\nu,{\rm syn}} \propto U_B(\gamma_{\rm e}) \gamma_{\rm e}^2 \, {\rm d}N_{\rm e}/{\rm d}\ln\gamma_{\rm e}$; using the scaling for $U_B(\gamma_{\rm e})$ given in equation (9), one recovers $\nu F_{\nu,{\rm syn}} \propto [1 + Y(\gamma_{\rm e})]^{-1} \gamma_{\rm e}^{2-p}$ indicated in equation (12). One can proceed similarly for the other two regimes, noting in particular that for $\gamma_{\rm m} < \gamma_{\rm e} < \gamma_{\rm c}$ (slow cooling), $U_B = U_{B-}$ and it no longer depends on $\gamma_{\rm e}$.

Finally, using the above electron distribution, one can compute the IC component using standard formulae:

$$F_{\nu,{\rm IC}}(\nu_{\rm IC}) \simeq \tau_{\rm IC} \int {\rm d}\gamma_{\rm e} \frac{1}{N_{\rm e}} \frac{{\rm d}N_{\rm e}}{{\rm d}\gamma_{\rm e}} \int_0^1 {\rm d}q \, (1-u) g_{\rm KN}(q)$$
$$\times F_{\nu,{\rm syn}} \left[\frac{\nu_{\rm IC}}{4\gamma^2 q(1-u)}\right] \Theta(1-u), \qquad (17)$$

with $u \equiv (1 + z)h\nu_{\rm IC}/(\Gamma_{\rm b}\gamma_{\rm e}m_{\rm e}c^2)$; the function $g_{\rm KN}(q) = [2q\ln q + (1 + 2q)(1 - q) + G^2(1 - q)/[2(1 + G)]]$, with $G \equiv u/(1 - u)$, characterizes the energy dependence of the KN cross-section, see Blumenthal & Gould (1970) for details.

The prefactor $\tau_{\rm IC}$ defines the optical depth to Compton scattering; an explicit calculation leads to

$$\tau_{\rm IC} = 3\sigma_{\rm T} \frac{N_{\rm e}}{4\pi r^2} = 12\sigma_{\rm T}\Gamma_{\rm b} n c t_{\rm dyn}. \qquad (18)$$

Note that this expression uses $N_{\rm e} = 4\pi r^2 \, ct_{\rm dyn} \, 4\Gamma_{\rm b} n$, i.e. it only includes the electrons that have been swept up in the last dynamical time-scale, because electrons injected at earlier times have been adiabatically cooled to Lorentz factors $< \gamma_{\rm c}$ and therefore do not participate in shaping the IC spectrum. With the above value of $\tau_{\rm IC}$, one can verify that the energy density of the radiation associated with the IC component is correctly normalized to $Y_{\rm c}$ times that contained in the synchrotron component, as can be verified by

calculating $\int {\rm d}\nu_{\rm IC} F_{\nu_{\rm IC},{\rm IC}}$ in terms of $\int {\rm d}\nu_{\rm syn} F_{\nu_{\rm syn},{\rm syn}}$ (neglecting the influence of KN effects).

2.4 Slow cooling

2.4.1 General procedure

As discussed in detail in Nakar et al. (2009) and Wang et al. (2010), the cooling Lorentz factors and Compton parameters $\gamma_{\rm c}$ and $Y_{\rm c}$ can be obtained in the slow-cooling regime $\gamma_{\rm m} < \gamma_{\rm c}$ from the system,

$$Y_{\rm c}(1 + Y_{\rm c}) \simeq \frac{\epsilon_{\rm e}}{\epsilon_{B-}} \left(\frac{\gamma_{\rm c}}{\gamma_{\rm m}}\right)^{2-p} \frac{U_{\rm syn}(< \tilde{\nu}_{\rm c})}{U_{\rm syn}(< \nu_{\rm c})}$$
$$\gamma_{\rm c} \simeq \frac{\gamma_{\rm c,syn}}{1 + Y_{\rm c}} \qquad (19)$$

with $\gamma_{\rm c,syn} \equiv (3/4)m_{\rm e}c/(\sigma_{\rm T} U_{B-} t_{\rm dyn})$ the cooling Lorentz factor in the relaxed turbulence, in the absence of IC losses.

Write $C_{\rm c} \equiv U_{\rm syn}(< \tilde{\nu}_{\rm c})/U_{\rm syn}(\nu_{\rm c})$ the term entering the first equation. If $\tilde{\nu}_{\rm c} < \nu_{\rm c}$, $C_{\rm c} < 1$ because the peak of the synchrotron flux lies at $\nu_{\rm c}$ or above (see below); in this limit, KN suppression inhibits the cooling of $\gamma_{\rm c}$ electrons. Assuming that such electrons cool by interacting with the $\nu_{\rm min} < \nu < \nu_{\rm c}$ part of the synchrotron spectrum, which is generically the case, one can write $C_{\rm c} = (\tilde{\nu}_{\rm c}/\nu_{\rm c})^{(3-p)/2} \propto \gamma_{\rm c}^{-3(3-p)/2}$ and the system can be solved easily.

In the opposite limit, $\tilde{\nu}_{\rm c} > \nu_{\rm c}$; one may have $C_{\rm c} \sim 1$ if the peak of the synchrotron flux is located at $\nu_{\rm c}$, or $C_{\rm c} \gtrsim 1$ if the peak lies at higher frequencies. In the latter case, $C_{\rm c} \simeq (\tilde{\nu}_{\rm c}/\nu_{\rm c})^{1-\beta}$, where β is the synchrotron spectral index defined by $F_{\nu,{\rm syn}} \propto \nu^{-\beta}$ in the spectral range above $\nu_{\rm c}$, calculated thereafter. The analytical calculation proposed here uses equation (27) below to derive this β, but the result depends little on this choice, because in all cases considered, $1 - \beta$ is small, meaning that the peak flux is not very different from the flux νF_ν at $\nu_{\rm c}$.

The next step is to determine the critical Lorentz factors $\widehat{\gamma}_{\rm c} \equiv \widehat{\gamma}(\nu_{\rm c})$ and $\widehat{\gamma}_{\rm m} \equiv \widehat{\gamma}(\nu_{\rm m})$ with the general definition (Nakar et al. 2009):

$$\widehat{\gamma}(\nu) = \frac{\Gamma_{\rm b} m_{\rm e} c^2}{(1 + z)h\nu}, \qquad (20)$$

which corresponds to the Lorentz factor for which electrons interact with photons of frequency ν at the onset of the KN regime. Note that $\nu_{\rm m}$ and $\nu_{\rm c}$ are to be calculated in the relaxed turbulence of strength δB_- in this slow-cooling regime. Using equations (9)–(11), one may then calculate the Compton parameters $Y(\widehat{\gamma}_{\rm c})$ and $Y(\widehat{\gamma}_{\rm m})$. Note also that the slow-cooling limit $\gamma_{\rm m} < \gamma_{\rm c}$ implies $\widehat{\gamma}_{\rm c} < \widehat{\gamma}_{\rm m}$.

Another critical Lorentz factor is γ_0, for which $Y(\gamma_0) = 1$. If $Y(\widehat{\gamma}_{\rm m}) > 1$, then $\widehat{\gamma}_{\rm m} < \gamma_0$, and γ_0 can be obtained by solving

$$\frac{Y(\gamma_0)\,[1 + Y(\gamma_0)]^{-\alpha_t/(1+\alpha_t)}}{Y(\widehat{\gamma}_{\rm m})\,[1 + Y(\widehat{\gamma}_{\rm m})]^{-\alpha_t/(1+\alpha_t)}} = \left[\frac{\tilde{\nu}(\gamma_0)}{\nu_{\rm m}}\right]^{4/3} \left(\frac{\gamma_0}{\gamma_{\rm m}}\right)^{\alpha_t/(1+\alpha_t)} \qquad (21)$$

which derives from equation (11). The latter equation assumes that $\tilde{\nu}(\gamma_0)$ lies in the spectral range between $\nu_{\rm a}$ (synchrotron self-absorption frequency) and $\nu_{\rm m}$, in general a very good approximation; it can be generalized to other cases without difficulty. If $Y(\widehat{\gamma}_{\rm m}) < 1$, then $\gamma_0 < \widehat{\gamma}_{\rm m}$; one can repeat the above exercise to derive γ_0, replacing the $4/3$ exponents with $(3 - p)/2$, which characterizes the spectral dependence of $\nu F_{\nu,{\rm syn}}$ between $\nu_{\rm m}$ and $\nu_{\rm c}$.

For improved accuracy, one may also determine the next-order critical Lorentz factor $\widehat{\gamma}_c \equiv \Gamma_b m_e c^2 / [(1+z)h\nu_{\mathrm{syn}}(\widehat{\gamma}_c)]$. Following a procedure similar to the above, one can derive $\nu(\widehat{\gamma}_c)$ and $Y(\widehat{\gamma}_c)$.

The following makes use of the short-hand notation: $\widehat{\nu} = \nu_{\mathrm{syn}}(\widehat{\gamma})$ for various critical Lorentz factors; similarly, $\nu_{\mathrm{syn}}(\gamma_0)$ is written ν_0 for commodity.

One can derive the power-law $1 - \beta'$ index of $\nu F_{\nu,\mathrm{syn}}$ as follows. Below ν_c, the scaling remains unchanged compared to the standard case because the cooling history does not influence the synchrotron spectrum, and the results will not be repeated here. Above ν_c, the spectral slope is determined by the scalings of $Y(\gamma)$, $\nu(\gamma)$ and $\nu F_{\nu,\mathrm{syn}} \propto (1+Y)^{-1} \gamma^{2-p}$ (equation 12). In particular, if $\tilde{\nu}(\gamma)$ lies in a spectral domain in which $\nu F_{\nu,\mathrm{syn}} \propto \nu^{1-\beta}$, below the peak of the synchrotron energy flux, then electrons of Lorentz factor γ cool by IC interactions with that portion of the synchrotron spectrum if $Y(\gamma) \gg 1$, in which case equations (9)–(11) lead to

$$Y \propto \gamma^{\alpha_t - (1-\beta)(1+\alpha_t)}$$

$$\nu \propto \gamma^{2-\beta\alpha_t/2}$$

$$t_{\mathrm{cool}} \propto \gamma^{-\beta}. \tag{22}$$

Assuming $\nu F_{\nu,\mathrm{syn}} \propto \nu^{1-\beta'}$ in the range of interest around $\nu(\gamma)$, and using the above scalings, one obtains directly

$$1 - \beta' = \frac{2 - p - \alpha_t + (1-\beta)(1+\alpha_t)}{2 - \alpha_t/2 + (1-\beta)\alpha_t/2}. \tag{23}$$

The limit $\beta \to 1$ recovers the case in which $\tilde{\nu}$ lies above the peak of the synchrotron flux, discussed previously.

2.4.2 Power-law segments

As mentioned above, the synchrotron spectrum at $\nu < \nu_c$ remains unaffected and it is not discussed here. At the upper end of the spectral range, i.e. $\nu_0 < \nu$, $Y(\gamma) < 1$ because of the KN suppression of electron cooling, which implies that $\nu F_{\nu,\mathrm{syn}} \propto \nu^{1-\beta'}$ with

$$1 - \beta' = \frac{2 - p}{2 - \alpha_t/[2(1+\alpha_t)]} \quad [\nu_0 < \nu] \tag{24}$$

as can be derived from equation (12) with $1 + Y \simeq 1$. This scaling also matches that derived by a full computation of the electron cooling history with negligible IC losses in Lemoine (2013). For $\alpha_t = 0$, one recovers of course the standard fast-cooling index $\beta' = p/2$.

In the range $\widehat{\nu}_m < \nu < \nu_0$, if it exists, the synchrotron spectrum is shaped by electrons with Lorentz factor γ such that $\widehat{\gamma}_m < \gamma < \gamma_0$, which thus cool by interacting with photons in the range $\nu < \nu_m$; one can therefore use equation (23) with $1 - \beta = 4/3$, so that

$$1 - \beta' \simeq \frac{5 - 3p/2 + \alpha_t/2}{3 + \alpha_t/4} \quad (\widehat{\nu}_m < \nu < \nu_0). \tag{25}$$

The limit $\alpha_t \to 0$ gives $\beta' = -2/3 + p/2$, which fits the results of Nakar et al. (2009) in this frequency range.

In the range $\max(\nu_c, \widehat{\nu}_c) < \nu < \min(\widehat{\nu}_m, \nu_0)$, the Lorentz factor of electrons shaping that part of the spectrum satisfies $\max(\gamma_c, \widehat{\gamma}_c) < \gamma < \min(\widehat{\gamma}_m, \gamma_0)$; hence, one can use equation (23) with $1 - \beta = (3-p)/2$, leading to

$$1 - \beta' \simeq \frac{7 - 3p + (1-p)\alpha_t}{4 + (1-p)\alpha_t/2}$$

$$\left[\max(\nu_c, \widehat{\nu}_c) < \nu < \min(\widehat{\nu}_m, \nu_0)\right]. \tag{26}$$

Note that $\widehat{\nu}_c < \nu_c$ is equivalent to $\tilde{\nu}_c < \nu_c$. Here as well, one recovers the index $\beta' = -3/4 + 3p/4$ derived in Nakar et al. (2009) in the limit $\alpha_t \to 0$.

If $\tilde{\nu}_c < \nu_c$, meaning $\widehat{\gamma}_c < \gamma_c$, the above completes the description of the spectrum. If, however, $\nu_c < \tilde{\nu}_c$, one needs to describe the intermediate range $\nu_c < \nu < \widehat{\nu}_c$. This range can actually be decomposed into two sub-ranges, as follows.

For $\widehat{\widehat{\nu}}_c < \nu < \widehat{\nu}_c$, the corresponding Lorentz factor verifies $\widehat{\widehat{\gamma}}_c < \gamma < \widehat{\gamma}_c$; hence, $\nu_c < \tilde{\nu} < \widehat{\nu}_c$. Consequently, the particle cools on the spectral range of $\nu F_{\nu,\mathrm{syn}}$ that it contributes to through synchrotron emission, so that one can use equation (23) with $\beta = \beta'$, giving

$$1 - \beta' \simeq \frac{-2 + 3\alpha_t + \left[4 + (4 - 8p)\alpha_t + \alpha_t^2\right]^{1/2}}{2\alpha_t}$$

$$(\widehat{\widehat{\nu}}_c < \nu < \nu_c) \tag{27}$$

and $1 - \beta' \simeq 0.12$ for $\alpha_t = -0.5, p = 2.3$, i.e. a slowly rising $\nu F_{\nu,\mathrm{syn}}$.

Finally, in the remaining range $\nu_c < \nu < \widehat{\nu}_c$, the particle cools on photons of frequency in the range $\widehat{\nu}_c < \tilde{\nu} < \tilde{\nu}_c$, for which $1 - \beta$ is given by equation (26) above. This leads to

$$1 - \beta' \simeq \frac{15 - 7p + \alpha_t(1-p)(10 - p + \alpha_t)/2}{8 + \alpha_t(1-p)(10 + \alpha_t)/4}. \tag{28}$$

One finds $1 - \beta' \simeq 0.09$ for $\alpha_t = -0.5$ and $p = 2.3$.

2.4.3 IC component

In principle, one can derive analytical approximations to the IC component using the above broken power-law approximations, folded over the particle distribution, as in equation (17) above. However, this appears rather intricate, given the number of potential power-law segments, in regard to the quality of the approximation that one can obtain; indeed, as discussed in detail in Sari & Esin (2001), folding over the distribution function generally introduces logarithmic departures, which smooth out the power-law segments and breaks. One can nevertheless describe the general features of this IC component in the slow-cooling regime as follows.

Below $\nu_{\mathrm{IC,m}} = 2\gamma_m^2 \nu_m$, the slope is that of $\nu F_{\nu,\mathrm{syn}}$ below ν_m, i.e. 4/3. For $\nu_{\mathrm{IC,m}} < \nu < \nu_{\mathrm{IC,c}}$ with $\nu_{\mathrm{IC,c}} = 2\gamma_c^2 \nu_c$, the slope of $\nu F_{\nu,\mathrm{IC}}$ is $(3-p)/2$, reflecting that of $\nu F_{\nu,\mathrm{syn}}$ in the corresponding range. Above $\nu_{\mathrm{IC,c}}$, the IC component reflects, up to the aforementioned logarithmic corrections, the slope of $\nu F_{\nu,\mathrm{syn}}$ above ν_c, which is generally close to flat or gently rising, see above.

Consequently, if the synchrotron spectrum has an extended range above ν_c where it is close to flat (i.e. $\beta \sim 1$), then one might have a close to flat IC component, at least up to the cut-off frequency defined as

$$\nu_{\mathrm{IC,KN}} = \gamma_c^2 \tilde{\nu}_c \tag{29}$$

corresponding to the boosting of $\tilde{\nu}_c$ photons at the onset of the KN regime by γ_c electrons. One can define another cut-off frequency, as follows:

$$\nu_{\mathrm{IC},\widehat{c}} = \widehat{\gamma}_c^2 \nu_c \tag{30}$$

which corresponds to the boosting of ν_c photons by electrons of Lorentz factor $\widehat{\gamma}_c$, at the onset of the KN regime. The ratio $\nu_{\mathrm{IC},\widehat{c}}/\nu_{\mathrm{IC,KN}}$ can be written as $\widehat{\gamma}_c/\gamma_c$; hence, the ordering of one with respect to the other depends on whether $\gamma < \widehat{\gamma}_c$ or not. In any case, the actual cut-off occurs at $\nu_{\mathrm{IC,KN}}$, while the presence of $\nu_{\mathrm{IC},\widehat{c}}$ may
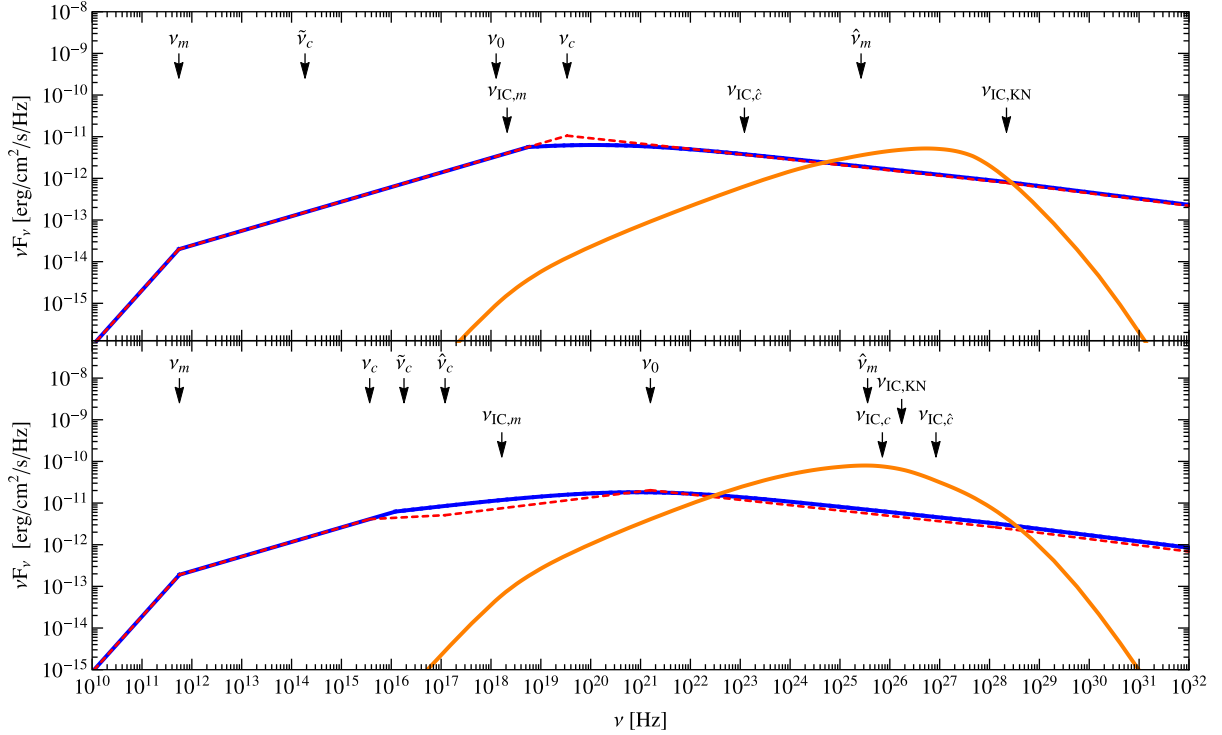
Figure 1. Comparison of the analytical calculation (dashed red line) of the synchrotron spectrum in the slow-cooling regime to a numerical calculation (solid blue line), for two representative cases: upper panel, observer time $t_{obs} = 10^4$ s, blast energy $E = 10^{53}$ erg, external density $n = 0.01$ cm^{-3}; lower panel, $t_{obs} = 3 \times 10^4$ s, $E = 10^{54}$ erg, $n = 10^{35} r^{-2}$ cm^{-3}; in both cases, $\epsilon_e = 0.1$, $p = 2.3$ and $\epsilon_B = \epsilon_{B+}[t/(100\omega_{pi}^{-1})]^{-0.4}$. The analytical estimates of the characteristic frequencies are indicated with arrows. The solid orange line represents the numerical calculation of the IC component.

lead to a feature (e.g. softening) in the IC spectrum. This can be understood by noting that in the present case, the synchrotron (energy) flux generically peaks above ν_c, while the particle distribution function falls steeply beyond γ_c; hence, the peak of the IC component is determined by the boosting of $\tilde{\nu}_c$ photons by electrons of Lorentz factor γ_c.

2.4.4 Comparison to numerical calculations

The above analytical broken power-law model of the synchrotron spectrum is compared to a full numerical calculation (with the algorithm described in Section 2.5 thereafter) in Fig. 1, in two different representative cases: upper panel, observer time $t_{obs} = 10^4$ s, blast energy $E = 10^{53}$ erg, external density $n = 0.01$ cm^{-3}; lower panel, $t_{obs} = 3 \times 10^4$ s, $E = 10^{54}$ erg, $n = 10^{35} r^{-2}$ cm^{-3} (wind profile with shock radius r expressed in cm); for both, $\epsilon_e = 0.1$, $p = 2.3$, $\epsilon_{B+} = 0.01$ and $\alpha_t = -0.4$, assuming $\epsilon_B = \epsilon_{B+}[t/(100\omega_{pi}^{-1})]^{\alpha_t}$. For a decelerating adiabatic Blandford & McKee (1976) solution, the value of the blast Lorentz factor at these observer times is $\Gamma_b \simeq 33$ in the upper panel and $\Gamma_b \simeq 29$ in the lower panel. For the above decay law of the magnetic field, one finds for the first scenario $\epsilon_{B-} = 3.2 \times 10^{-5}$ ($t_{dyn} = 1.3 \times 10^6$ s, $\omega_{pi}^{-1} = 7.6 \times 10^{-3}$ s), and in the second scenario $\epsilon_{B-} = 2.1 \times 10^{-5}$ ($t_{dyn} = 1.7 \times 10^6$ s, $\omega_{pi}^{-1} = 3.5 \times 10^{-3}$ s).

The critical frequencies are indicated with arrows. The thick solid line corresponds to the numerical calculation (synchrotron in blue, IC component in orange), while the dashed line shows the analytical estimates, which clearly provides a faithful match in both cases.

In the first scenario (upper panel), $\widehat{\gamma}_c \simeq 60$ while $\gamma_c \simeq 10^7$: KN effects are therefore particularly strong; they are actually so strong that $\nu_0 < \nu_c$, which means that the KN suppression of electron cooling reduces the Compton parameter to below unity at γ_c. Consequently, the dependence of Y on γ does not affect the spectrum above ν_c. Noting that in this region $\nu F_\nu \propto \gamma^{2-p}$ (equation 12) and $\nu \propto \gamma^{2-\alpha_t/2(1+\alpha_t)}$ (equation 10), one finds $\nu F_\nu \propto \nu^{1-\beta}$ with $1 - \beta = (2-p)/[2 - \alpha_t/2(1 + \alpha_t)]$, which matches equation (24). As mentioned earlier, the spectrum remains unaffected with respect to the standard synchrotron spectrum below ν_c because the electrons shaping that part of the spectrum do not cool on a dynamical time-scale.

In this first scenario, the method proposed in equations (19) overestimates γ_c by a factor of 2.5, hence ν_c by a factor of 6 and $\nu_{IC,KN} = \tilde{\nu}_c\gamma_c^2$ by a factor of 2.5 as well. Taking into account this overestimate, the numerical calculation indicates that the suppression of the IC flux becomes noticeable at a factor of ~5 below the theoretical value of $\nu_{IC,KN}$, as calculated with the correct γ_c. As anticipated, the characteristic frequency $\nu_{IC,\widehat{c}}$ leads to a soft softening in the IC component, but not to a cut-off.

In the second scenario (lower panel), $\gamma_c < \widehat{\gamma}_c$; hence, KN suppression of the IC cooling becomes effective at $\widehat{\nu}_c$ only. The (analytical) synchrotron spectrum is thus close to flat in the region $\nu_c \lesssim \nu \lesssim \widehat{\nu}_c$, as indicated by equations (27) and (28) above, then rising with $1 - \beta \simeq 0.14$ corresponding to equation (26) above for the range $\widehat{\nu}_c < \nu < \nu_0$, because $\nu_0 < \nu_m$. Above ν_0, equation (24) applies and gives the same high-energy spectral slope as for the previous scenario.

In this second case, the analytical calculations underestimate γ_c by a factor of 1.8. There is nevertheless broad satisfactory agreement
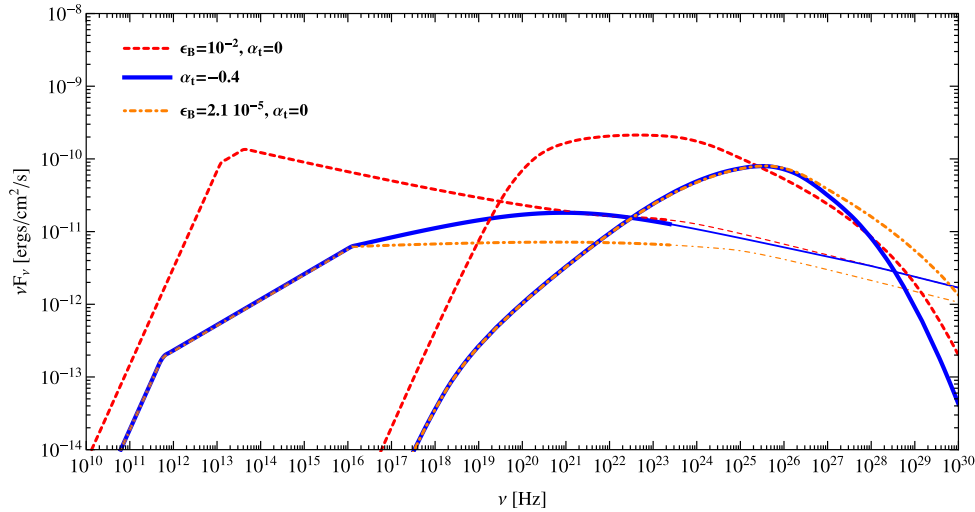
Figure 2. Synchrotron and IC spectra at $t_{obs} = 3 \times 10^4$ s, representative of the slow-cooling regime, for a blast with energy $E = 10^{54}$ erg impinging on a progenitor wind with density $n = 10^{35} \, r^{-2} \, \mathrm{cm}^{-3}$ (r in cm), assuming $\epsilon_e = 0.1$ and $p = 2.3$, for three microphysical models, as indicated: homogeneous (non-decaying) $\epsilon_B = \epsilon_{B+} = 0.01$ (dashed red line); decaying $\epsilon_B = \epsilon_{B+}[t/(100\omega_{pi}^{-1})]^{-0.4}$ (solid blue); homogeneous $\epsilon_B = \epsilon_{B-} = 2.1 \times 10^{-5}$ (dash–dotted orange), the value of ϵ_{B-} being representative of ϵ_B close to the contact discontinuity in the decaying ϵ_B model. The synchrotron model predictions have been thinned beyond an ad hoc maximal synchrotron photon energy of 1 GeV (see the text). Characteristic frequencies are for $\alpha_t = -0.4$ and for $\epsilon_B = \epsilon_{B-}$, $\nu_m \simeq 5.6 \times 10^{11}$ Hz, $\nu_c \simeq 1.2 \times 10^{16}$ Hz and $\nu_{IC, KN} \simeq 2 \times 10^{26}$ Hz; for $\epsilon_B = \epsilon_{B+}$, $\nu_m \simeq 1.2 \times 10^{13}$ Hz, $\nu_c \simeq 4.2 \times 10^{13}$ Hz and $\nu_{IC, KN} \simeq 2 \times 10^{24}$ Hz.

between the analytical synchrotron spectrum and the numerical calculation.

2.4.5 Comparison to non-decaying scenarios

Fig. 2 provides a numerical comparison of the spectra shown in the lower panel of Fig. 1 with two calculations for the same parameters but a homogeneous (non-decaying) turbulence: one in which $\epsilon_B = \epsilon_{B+} = 0.01$, another one in which $\epsilon_B = \epsilon_{B-} = 2.1 \times 10^{-5}$, which corresponds to the value of $\epsilon_B(t_{dyn})$, i.e. close to the contact discontinuity, in the above decaying microturbulence model.

As expected, the SSC spectrum with decaying microturbulence merges with that corresponding to uniform ϵ_{B-} at frequencies below ν_c, since electrons of Lorentz factor $\gamma < \gamma_c$ then cool in magnetized turbulences of equal strength in both models. The synchrotron spectrum for decaying microturbulence also merges with the synchrotron spectrum for uniform ϵ_{B+} at the highest frequencies, since the cooling time for those emitting electrons becomes shorter than Δ; hence, the particles effectively cool in a magnetic field characterized by ϵ_{B+}. However, the integrated powers for these two models differ, because the cooling efficiencies $\sim (\gamma_c/\gamma_m)^{2-p}$ differ.

In this regard, the slow-cooling synchrotron spectrum for decaying microturbulence is a hybrid of the spectra for uniform high and low ϵ_B, transiting from ϵ_{B-} at low frequencies to ϵ_{B+} at high frequencies. This justifies the use of a two-zone model, one with low ϵ_{B-} and one for high ϵ_{B+}, to compute an approximated spectrum in wavebands at respectively low and high frequencies.

In Fig. 2, the synchrotron spectra have been arbitrarily continued at very high frequencies, albeit with a thin line, but they should of course cut off at some maximal energy where the acceleration time-scale becomes of the same order as the cooling time-scale. Since this depends on acceleration physics, see the discussion in Lemoine (2013), the lines have been turned from thick to thin at an ad hoc location corresponding to a synchrotron photon energy of 1 GeV. This estimate is discussed in Plotnikov et al. (2013), Lemoine

(2013), Wang et al. (2013) and Sironi et al. (2013); it depends on the afterglow parameters and, in particular, on observer time.

For reference, one notes the critical frequencies:

$$
\nu_{IC,c} = 2\gamma_c^2 \nu_c
$$
$$
\simeq 7.3 \times 10^{23} \, \mathrm{Hz} \, E_{54} \epsilon_{B-,-5}^{-7/2} A_{\star,11.7}^{-9/2} t_{obs,4.5}^2 z_+^{-3} Y_{c,2}^{-4}
$$
$$
\nu_{IC,KN} = \frac{1}{1+z}\Gamma_b \gamma_c m_e c^2
$$
$$
\simeq 4 \times 10^{25} \, \mathrm{Hz} \, E_{54}^{1/2} \epsilon_{B-,-5}^{-1} A_{\star,11.7}^{-3/2} t_{obs,4.5}^{1/2} z_+^{-3/2} Y_{c,2}^{-1} \quad (31)
$$

with the notations $z_+ = (1+z)/2$, $Y_{c,2} = (1+Y_c)/100$ and $A_{\star,11.7} = A_\star/(5 \times 10^{11} \, \mathrm{g \, cm}^{-2})$. For reference, in the scenario of Figs 2 and 3, $A_\star \simeq 0.3$ and $Y_c \simeq 50$ for $\epsilon_{B-} = 2.1 \times 10^{-5}$. Note the strong dependence of $\nu_{IC,c}$ and ν_{KN} on the external density. As discussed above, the peak of the IC component is expected to occur at $\nu_{IC,KN}$, although the numerical calculation suggests that the turn-over becomes manifest a factor of ~ 5 below the above theoretical value.

The VERITAS collaboration has recently been able to observe the exceptional GRB130427A and to put stringent upper limits on the emission at $\gtrsim 100$ GeV (Aliu et al. 2014). The absence of detection of this energy range suggests that, for this burst at least, the IC component has cut-off below $\simeq 100$ GeV, while the Fermi detection of multi-GeV photons up to a day or so suggests that this cut-off lied above 1–10 GeV. Such a cut-off energy fits well with the above estimates for $\nu_{IC,KN}$ for a low average ϵ_B.

2.5 Fast cooling

The fast-cooling regime involves a substantial variety of synchrotron spectra, with multiple breaks and indices, as discussed in detail in Nakar et al. (2009) and Wang et al. (2010) for the case of uniform ϵ_B. One key difference with the slow-cooling regime is that particles with Lorentz factors $\gamma < \max(\gamma_c, \gamma_m)$ may have a non-trivial cooling history while in the slow-cooling regime, such particles do not cool. As a consequence, it is difficult to even derive
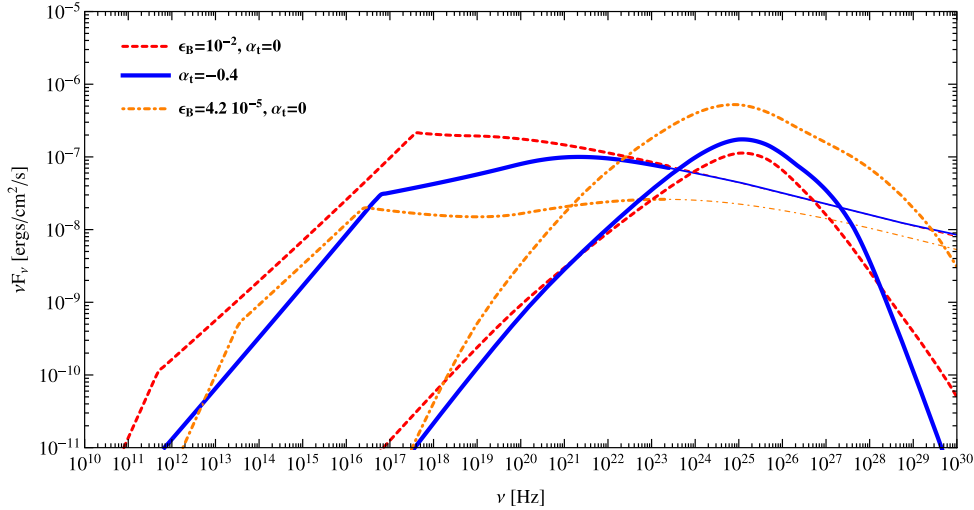
Figure 3. Same as Fig. 2 at observer time $t_{obs} = 30\,s$, representative of the fast-cooling regime. Characteristic frequencies are for $\alpha_t = -0.4$, $\nu_c \simeq 10^{12}$ Hz, $\nu_m \simeq 3 \times 10^{16}$ Hz and $\gamma_m^2 \tilde{\nu}_m \simeq 6 \times 10^{25}$ Hz; for $\epsilon_B = \epsilon_{B-}$, $\nu_c \simeq 2 \times 10^{13}$ Hz, $\nu_m \simeq 3 \times 10^{16}$ Hz and $\gamma_m^2 \tilde{\nu}_m \simeq 6 \times 10^{25}$ Hz; for $\epsilon_B = \epsilon_{B+}$, $\nu_c \simeq 4 \times 10^{11}$ Hz, $\nu_m \simeq 4 \times 10^{17}$ Hz and $\gamma_m^2 \tilde{\nu}_m \simeq 6 \times 10^{25}$ Hz.

the cooling Lorentz factor and the Compton parameter Y_c when KN effects become significant.

In this fast-cooling regime, it is actually more efficient to compute the spectrum numerically, using the following simple and efficient algorithm. One starts with a template synchrotron spectrum, for instance that corresponding to a homogeneous magnetized turbulence. One can then derive a first approximation to γ_c and Y_c, either using standard formulae (e.g. Panaitescu & Kumar 2000) – which ignore KN effects – or through an explicit determination of γ_c as the Lorentz factor for which cooling takes place on a dynamical time-scale, using a radiation energy density inferred from the template spectrum. With γ_c and Y_c, one can solve equations (9)–(11) to compute the frequencies and Compton parameter as a function of the initial Lorentz factor of an electron; one can then use equations (12) and (13) to compute an improved version of the synchrotron spectrum, properly taking into account the cooling history of the electrons in the decaying turbulence as well as all relevant KN effects. The latter spectrum remains an approximation, because it relies on a guessed value for γ_c and Y_c. Nevertheless, iterating the above process, using each time as a template the previously computed synchrotron spectrum, one obtains after ~ 10 iterations a self-consistent synchrotron spectrum, with γ_c and Y_c determined to high accuracy. Finally, one can derive the IC spectrum using equation (17).

The above algorithm provides a self-consistent estimate of the synchrotron and IC spectra with a normalization accuracy of order unity. This accuracy can be checked by calculating a posteriori the integrated synchrotron and IC powers and comparing to the total electron power injected through the shock: in the fast-cooling regime, these should match. The error is of the order of 10–40 per cent for the SSC spectrum of a decaying microturbulence as shown in Fig. 3, depending on observer time; it is less than 10–20 per cent for $\alpha_t = 0$ and $\epsilon_B = \epsilon_{B+}$, but it becomes a factor of $\lesssim 2$ for $\alpha_t = 0$ and $\epsilon_B = \epsilon_{B-}$. Most of the error results from the broken power-law normalization of the flux in equation (12) and from the treatment of the KN cross-section as a step function in the calculation of the synchrotron cooling history. The resulting uncertainty remains nevertheless satisfactory given the uncertainty

associated for instance with the definition of t_{dyn} (hence γ_c) in the absence of a realistic description of the blast energy profile.

A detailed example of the SSC spectrum of the blast, for the same parameters as in Fig. 2, is presented in Fig. 3 at an observer time $t_{obs} = 30\,s$; assuming a Blandford & McKee (1976) decelerating solution in a wind profile, the Lorentz factor of the blast at that time is $\Gamma_b \simeq 160$. The value of ϵ_{B-} in this case is 4.2×10^{-5}. As expected, the spectrum corresponding to a decaying turbulence merges with the spectrum for uniform $\epsilon_B = \epsilon_{B+}$ above a frequency $\nu \sim 10^{23}$ Hz, since the electrons that emit in that range cool fast, in a region where $\epsilon_B \simeq \epsilon_{B+}$. In this fast-cooling regime, the total integrated energy densities of the three SSC spectra correspond to the injected electron energy density. The spectrum for decaying microturbulence does not merge with that for uniform $\epsilon_B = \epsilon_{B-}$ at low frequencies, since the cooling Lorentz factors differ for both. In this fast-cooling regime, one cannot therefore describe accurately the synchrotron spectrum at low frequencies with a spectrum computed for uniform low ϵ_B: an explicit calculation becomes necessary.

Finally, note that the IC component in the fast-cooling regime is expected to peak at $\gamma_m^2 \nu_m$, if the synchrotron flux peaks at ν_m and if one omits KN effects. The KN suppression implies a turn-over of the IC component at most at $\gamma_m^2 \tilde{\nu}_m$, for reasons analogous to those discussed in the slow-cooling regime, see also Nakar et al. (2009). If $\nu_m < \tilde{\nu}_m$, the slow rise of the synchrotron flux above ν_m in the case of low ϵ_B (due to the KN suppression of electron cooling) or decaying microturbulence implies a comparable behaviour of the IC component between $\gamma_m^2 \nu_m$ and $\gamma_m^2 \tilde{\nu}_m$. This feature is not clearly seen in Fig. 3 due to the (relative) proximity of these two frequencies, $\gamma_m^2 \tilde{\nu}_m \simeq 6 \times 10^{25}$ Hz and $\gamma_m^2 \nu_m \simeq 10^{24}$ Hz.

3 SPECTRA AND LIGHT CURVES

3.1 Spectral and temporal behaviours

The spectra shown in Figs 2 and 3 illustrate how a complete and simultaneous spectral coverage would allow one to tomograph the evolution of the microturbulence behind the relativistic shock. The effects are most noticeable in the X-ray and MeV regions, as one

would expect: in this region of the spectrum, the emitting electrons feel the decaying turbulence, while at the highest frequencies, they cool in regions with $\epsilon \sim \epsilon_{B+}$, and at frequencies $\nu < \nu_c$ they cool in a magnetic field characterized by ϵ_{B-}, the value of which evolves slowly in time.

Afterglow models often rely on the spectral and temporal slopes in various domains and their so-called closure relations to make comparison to observations. Fig. 4 therefore presents the spectral slopes β defined by $F_\nu \propto \nu^{-\beta}$ (where F_ν sums the synchrotron and IC fluxes), for the optical, X-ray, high-energy (0.1–10 GeV) and very high energy (>10 GeV) ranges (note that no attenuation in extragalactic background radiation has been assumed for the latter range). This figure compares the spectral slopes for the three previous representative models: ($\alpha_t = 0$, $\epsilon_B = 0.01$), $\alpha_t = -0.4$ and ($\alpha_t = 0$, $\epsilon_B = 10^{-5}$) with otherwise same parameters as in Figs 2 and 3, except k, which takes values 0 (constant-density profile) or 2 (stellar wind).

In the optical, β has been calculated at a reference frequency of 4.7×10^{14} Hz (R band); in the X-ray, β is calculated as the average slope over the interval of energies 0.3–10 keV; at high energy, it is calculated as the average of the energy interval 0.1–10 GeV and at very high energy, over >10 GeV.

According to Fig. 4, the most robust signature of a decaying microturbulence appears to be a slightly harder slope in the X-ray, $\beta \simeq 0.9$ [panels (b) and (e)] versus $\beta \simeq 1.15$ for uniform ϵ_B in the first hours [panels (a), (c), (d) and (f)]. The latter value corresponds to the fast-cooling regime $\beta = p/2$; therefore, it depends on p. However, one does not expect it to go below 1, because $p > 2$ is a generic prediction of relativistic shock acceleration, e.g. Bednarz & Ostrowski (1998), Kirk et al. (2000), Achterberg et al. (2001), Lemoine & Pelletier (2003) and Sironi et al. (2013). Current data do not allow one to distinguish between these limits; in particular, the *Swift* data lead to $\beta \simeq 1 \pm 0.1$ (Evans et al. 2009) in afterglows with standard power-law decay. Interestingly, even in the case of a homogeneous turbulence, the X-ray slope hardens at late times because of the emergence in the X-ray range of the IC component; for instance, in panels (a) and (c), one can see β transits to values of the order of 0.7, corresponding to the low-energy extension of this IC component with slope $\beta = (p-1)/2$.

In the optical range, the slope is comparable to that in the X-ray range for the decaying microturbulence scenario at observer times $\sim 10^3$ s, but significantly harder at earlier times when the optical falls in the range $\nu_c - \nu_m$: Fig. 4 indicates values $\beta \sim 0.3$, harder than expected (1/2) in the standard fast-cooling regime in this range of frequencies. At an observer time $t_{obs} = 30$ s, for $k = 2$ corresponding to panel (e) as well as to Fig. 3, $\tilde{\nu}_m \simeq 1.4 \times 10^{18}$ Hz, which lies below the peak of the synchrotron component (see Fig. 3). This implies that KN effects are significant, and that γ_m electrons cool by interacting with the segment in the range 10^{17}–10^{21} Hz, whose index $\beta \sim 0.8$. In this case, one can compute the expected index β' of the segment below ν_m, using a variant of equation (23): one notes that $\nu F_{\nu,\mathrm{syn}} \propto \gamma/(1 + Y)$ (equation 13), which gives

$$1 - \beta' = \frac{1 - \alpha_t + (1 - \beta)(1 + \alpha_t)}{2 - \alpha_t/2 + (1 - \beta)\alpha_t/2} \simeq 0.3, \qquad (32)$$

the last equality applying for $\alpha_t = -0.4$ and $\beta = 0.8$. This explains the values of α_t found in the optical range. Such values do depart from the standard synchrotron spectra, although KN effects may also cause values $\beta \sim 0.3$ below ν_{min} in the case of homogeneous turbulence scenarios, see Nakar et al. (2009), their figs 2 and 3 for example. Therefore, it is not clear at present whether
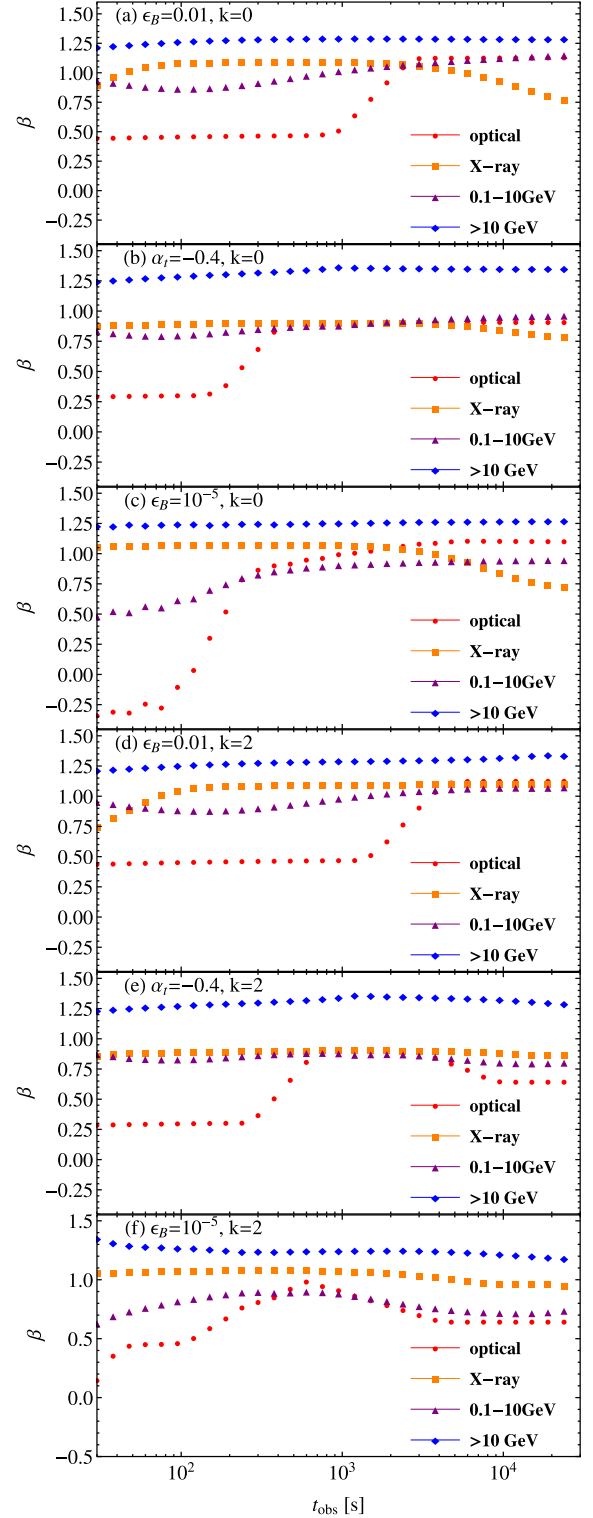
Figure 4. Flux density index β, with $F_\nu \propto \nu^{-\beta}$, as a function of time, in various wavebands, for different external density profiles: $k = 2$ (wind, $n = 10^{35} r^{-2}$ cm^{-3}) and $k = 0$ (constant density, $n = 1$ cm^{-3}), assuming uniform $\epsilon_B = 0.01$, $\epsilon_B = (100\omega_{pi})^{\alpha_t}$ or uniform $\epsilon_B = 10^{-5}$. Blast energy, jet Lorentz factor and ϵ_e are as in Fig. 2. Wavebands are as indicated: for reference, optical (circles) $\nu = 4.7 \times 10^{14}$ Hz, X-ray (squares) integrated from 0.3 to 10 keV (i.e. 0.72–24 $\times 10^{17}$ Hz), 0.1–10 GeV (upward triangles, in frequency 0.24–24 $\times 10^{23}$ Hz) and > 10 GeV (diamonds, in frequency $> 24 \times 10^{23}$ Hz).

one can consider such values of β as a clear signature of a decaying microturbulence.

All in all, an accurate measurement of β in the X-ray range or, better, in the MeV range if the MeV afterglow could be detected would provide the best probe of α_t, see also Figs 2 and 3 for illustrations of these effects.

Another quantity of interest for a general description of the afterglow is the temporal slope, defined by $F_\nu \propto t_{\mathrm{obs}}^{-\alpha}$. Of course, these temporal slopes directly depend on the time evolution of the various parameters, through the assumed evolutionary law for Γ_{b} and the evolution of r and n, in contrast to the spectral slopes β at any given time. Here Γ_{b} is assumed to decrease as in the Blandford & McKee (1976) adiabatic solution, i.e. $\Gamma_{\mathrm{b}} \propto t^{(k-3)/[2(4-k)]}$.

The values of α for the same models and intervals as Fig. 4 are reported in Fig. 5. The largest differences between constant (high) and decaying ϵ_B result from the different transit times between the slow- and fast-cooling regimes, but these times depend in turn on other parameters that are a priori unknown. The light curves otherwise present similar features, without a clear trend distinguishing one from the other.

Figs 4 and 5 thus indicate that α and β are by themselves weakly sensitive probes of the dynamics of the magnetized turbulence in the blast and that it is not possible at present to distinguish a decaying microturbulence from a uniform low or high ϵ_B on the basis of these data. It appears much more effective to try to probe ϵ_B through a multiwavelength fit of the afterglow light curves, using not only the temporal and spectral slopes, but also the ratio of fluxes between different spectral windows, as done in Lemoine et al. (2013) and Liu, Wang & Wu (2013) for *Fermi*-LAT bursts.

3.2 Emission at very high energy

Finally, an interesting consequence of a decaying microturbulence is the generic prediction of substantial emission at the highest energies, due to the large value of the Compton parameter. Naive estimates, $Y \sim \sqrt{\epsilon_e/\epsilon_{B-}}$, indicate values of several hundreds for Y, although they neglect KN effects which depend on the electron energy, therefore on observed frequency; furthermore, the non-trivial spectral shape above ν_c in the case of decaying microturbulence modifies the ratio of the IC to the synchrotron component. As discussed in Wang et al. (2013), emission above 10 GeV is most likely of IC origin, because the maximal synchrotron photon energy is more likely of the order of 1 GeV or so at 100–1000 s observer time. This emission is a prime target for future gamma-ray telescopes such as HAWK (Mostafa 2013) or CTA (Inoue et al. 2013). For the particular case of CTA, Inoue et al. (2013) have investigated the detection rates of GRBs above 30 GeV by assuming that the spectrum continues beyond 1 GeV with a spectral index $\beta = 1.1$ (corresponding to the standard fast-cooling regime $\beta = p/2$ with $p = 2.2$) and scaling the flux at 1 GeV to that measured by the *Fermi*-LAT instruments. Their simulations lead to about one detection per year. This rate is rather low; therefore, any improvement would be quite valuable, given the potential impact of a high-energy detection.

One can use the calculations of Section 2 to study how a decaying microturbulence or low ϵ_{B-} affects these predictions. In order to do so, one calculates the ratio of the total (synchrotron + IC) energy flux above 30 GeV, $F(>30\,\mathrm{GeV}) = \int_{30\,\mathrm{GeV}} F_\nu \, \mathrm{d}\nu$, to a theoretical reference flux $F_{\mathrm{th}}(>30\,\mathrm{GeV})$. As in Inoue et al. (2013), $F_{\mathrm{th}}(>30\,\mathrm{GeV})$ is obtained by extrapolating the total flux measured at a reference
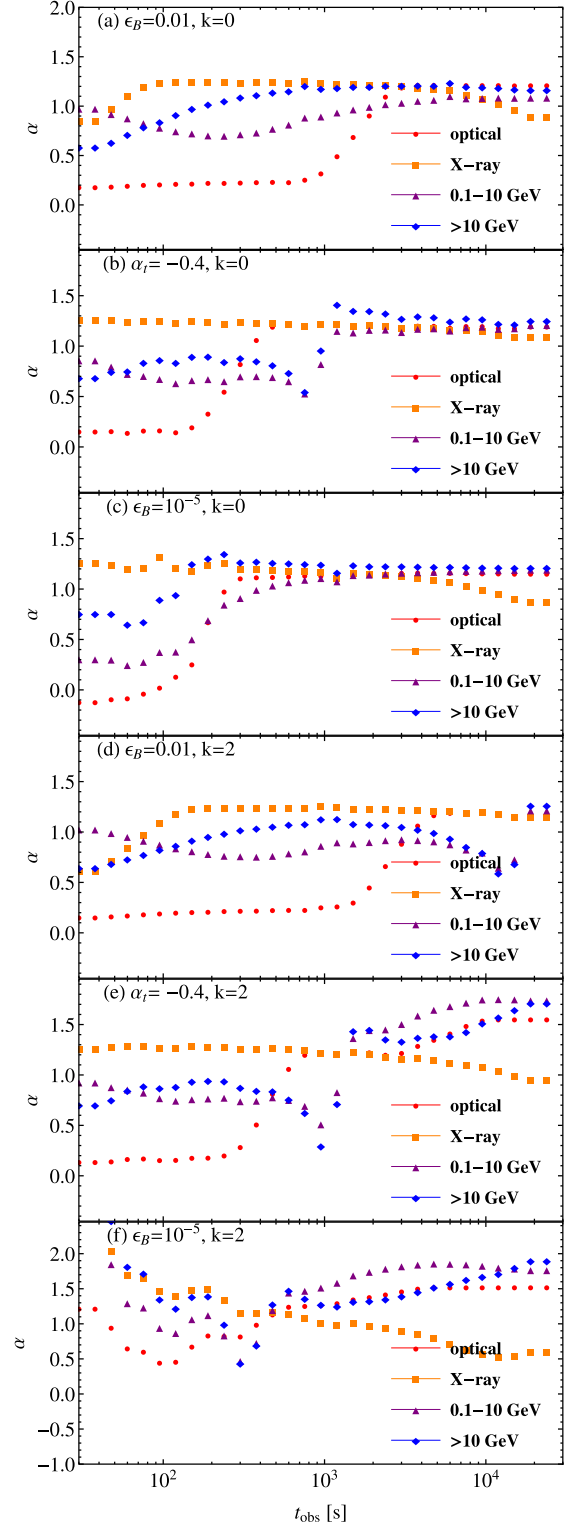
Figure 5. Observer time decay index of the flux density, i.e. $F_\nu \propto t_{\mathrm{obs}}^{-\alpha}$, for various models, as indicated in Fig. 4. Blast energy and ϵ_e are as in Fig. 2.

energy, here 0.1 GeV, with an index $\beta \simeq 1.1$, i.e.

$$F_{\mathrm{th}}(>30\,\mathrm{GeV}) = F_\nu(0.1\,\mathrm{GeV})$$

$$\times \int_{30\,\mathrm{GeV}/h}^{+\infty} \mathrm{d}\nu \left(\frac{h\nu}{0.1\,\mathrm{GeV}} \right)^{-1.1} \tag{33}$$
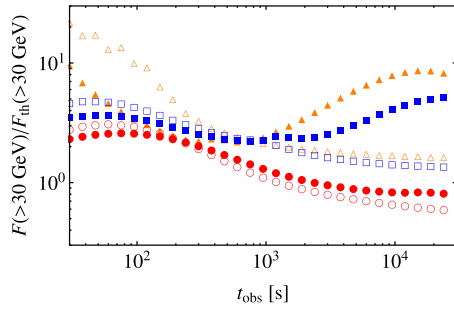
Figure 6. Ratio of the total energy flux above 30 GeV to a theoretical flux obtained by matching the calculated total flux at 0.1 GeV and extrapolating this flux to higher energies with a power law $F_{\nu,\mathrm{th}} \propto \nu^{-1.1}$, as in Inoue et al. (2013). The symbols correspond to the six models studied in Figs 4 and 5, as follows: red circles $\epsilon_B = \epsilon_{B+}$ and $\alpha_t = 0$; blue squares $\alpha_t = -0.4$; orange triangles $\epsilon_B = \epsilon_{B-}$ and $\alpha_t = 0$. Filled symbols correspond to $k = 2$ and open symbols to $k = 0$; other parameters are as in Fig. 2.

with $F_\nu = F_{\nu,\mathrm{syn}} + F_{\nu,\mathrm{IC}}$ the total flux. The reference energy chosen here is smaller than that in Inoue et al. (2013), because the IC flux is already prominent at 1 GeV in the scenarios studied, as shown in Figs 2 and 3 for example. However, given the value of the index β, the theoretical flux νF_ν is roughly flat above 1 GeV; hence, this should not affect the statistics of detection.

The results are shown in Fig. 6, which carries out this evaluation for the six models shown in Figs 4 and 5. This figure indicates that a decaying microturbulence with $\alpha_t = -0.4$ (or a low average ϵ_B) increases by a factor of a few, up to an order of magnitude, depending on α_t, k and t_{obs}, the prospects of observing the afterglows at energies >30 GeV, relatively to statistics computed for a model with $\epsilon_B = 0.01$, as in Inoue et al. (2013). This certainly brings the number of potential detections by instruments such as CTA in a more comfortable range.

Furthermore, it is important to note that in most models studied here, the IC component contributes to a significant fraction of the total flux at 0.1 GeV; therefore, the above ratio actually is an underestimate of the ratio of the IC flux at high energies to the synchrotron flux at GeV energies.

4 CONCLUSIONS

This paper has discussed the spectral shapes of the SSC spectrum of a relativistic blast wave, including all relevant KN effects, and their evolution in time. A particular emphasis has been put on the impact of a decaying microturbulence behind the shock front, which is motivated by theoretical analysis (Chang et al. 2008; Lemoine 2015) and observational inference (Lemoine et al. 2013; Liu et al. 2013). However, the results are fully applicable to the case of a uniformly magnetized blast, possibly with a low value of the average ϵ_B.

A decaying microturbulence and/or a low average value of ϵ_B both lead to a large Y_c Compton parameter, with interesting physical and observational consequences. From a more theoretical point of view, the KN suppression of IC cooling has a strong effect on the synchrotron spectral shape, as noted elsewhere for the case of a uniformly magnetized blast (Nakar et al. 2009; Wang et al. 2010). In the case of a decaying microturbulence, the modification is not trivial to compute, and the present paper has described a simple algorithm which allows one to compute the full SSC spectrum with satisfactory accuracy, at a modest numerical cost. Among the interesting phenomenological consequences, one may point out the slight deviations in the spectral and temporal slopes induced by the

decaying microturbulence, or by KN effects in uniformly magnetized blasts at low ϵ_B. A multiwavelength coverage of the afterglow would, in principle, allow one to tomograph the dynamics of this magnetized turbulence, through its influence on the light curves in various wavebands. However, as expressed in terms of the spectral β and temporal α slopes, defined customarily through $F_\nu \propto t_{\mathrm{obs}}^{-\alpha} \nu^{-\beta}$, the deviations are relatively weak and not currently distinguishable through observations. A multiwavelength fit of the afterglow, which also relies on the flux ratios between various wavebands, seems to provide a more sensitive probe of the dynamics of the microturbulence.

Finally, a large Y_c parameter also implies a large IC flux at multi-GeV energies, relatively to the lower energy synchrotron flux, with direct consequences for the detectability of GRB afterglows by future gamma-ray telescopes. A numerical estimate indicates that a low average ϵ_B would imply a detection rate several times larger than currently anticipated on the basis of the extrapolation of the flux of GRBs detected by *Fermi*-LAT.

REFERENCES

Achterberg A., Wiersma J., 2007, A&A, 475, 19
Achterberg A., Gallant Y. A., Kirk J. G., Guthmann A. W., 2001, MNRAS, 328, 393
Achterberg A., Wiersma J., Norman C. A., 2007, AA, 475, 1
Aliu E. et al., 2014, ApJ, 795, L3
Barniol-Duran R., 2014, MNRAS, 443, 3578
Barniol-Duran R., Kumar P., 2011, MNRAS, 417, 1584
Bednarz J., Ostrowski M., 1998, Phys. Rev. Lett., 80, 3911
Blandford R. D., McKee C. F., 1976, Phys. Fluids, 19, 1130
Blumenthal G. R., Gould R. J., 1970, Rev. Mod. Phys., 42, 237
Bošnjak Ž, Daigne F., Dubus G., 2009, A&A, 498, 677
Bret A., Gremillet L., Bénisti D., 2010, Phys. Rev. E, 81, 036402
Chang P., Spitkovsky A., Arons J., 2008, ApJ, 674, 378
Daigne F., Bošnjak Ž, Dubus G., 2011, AA, 526, 110
Derishev E., 2007, Ap&SS, 309, 157
Evans P. A. et al., 2009, MNRAS, 397, 1177
Gruzinov A., Waxman E., 1999, ApJ, 511, 852
Haugbølle T., 2011, ApJ, 739, 42
He H.-N., Wu X.-F., Toma K., Wang X.-Y., Mészáros P., 2011, ApJ, 733, 22
Inoue S. et al., 2013, Astropart. Phys., 43, 252
Kato T. N., Takabe H., 2008, ApJ, 681, L93
Keshet U., Katz B., Spitkovsky A., Waxman E., 2009, ApJ, 693, L127
Kirk J., Reville B., 2010, ApJ, 710, 16
Kirk J., Guthmann A. W., Gallant Y., Achterberg A., 2000, ApJ, 542, 235
Kumar P., Barniol-Duran R., 2009, MNRAS, 400, L75
Kumar P., Barniol-Duran R., 2010, MNRAS, 409, 226
Lemoine M., 2013, MNRAS, 428, 845
Lemoine M., 2015, J. Plasma Phys., 81, 455810101
Lemoine M., Pelletier G., 2003, ApJ, 589, L73
Lemoine M., Pelletier G., 2010, MNRAS, 402, 321
Lemoine M., Pelletier G., 2011, MNRAS, 417, 1148
Lemoine M., Pelletier G., Revenu B., 2006, ApJ, 645, L129
Lemoine M., Li Z., Wang X.-Y., 2013, MNRAS, 435, 3009
Lemoine M., Pelletier G., Gremillet L., Plotnikov I., 2014a, Europhys. Lett., 106, 55001
Lemoine M., Pelletier G., Gremillet L., Plotnikov I., 2014b, MNRAS, 440, 1365

Liu R.-Y., Wang X.-Y., Wu X.-F., 2013, ApJ, 773, L20
Lyubarsky Y., Eichler D., 2006, ApJ, 647, L1250
Martins S. F., Fonseca R. A., Silva L. O., Mori W. B., 2009, ApJ, 695, L189
Medvedev M. V., Loeb A., 1999, ApJ, 526, 697
Moiseev S. S., Sagdeev R. Z., 1963, J. Nucl. Energy, 5, 43
Mostafa M., 2013, preprint (arXiv:1310.7237)
Nakar E., Ando S., Sari R., 2009, ApJ, 703, 675
Niemiec J., Ostrowski M., Pohl M., 2006, ApJ, 650, 1020
Nishikawa K.-I. et al., 2009, ApJ, 698, L10
Panaitescu A., Kumar P., 2000, ApJ, 543, 66
Pelletier G., Lemoine M., Marcowith A., 2009, MNRAS, 393, 587
Piran T., 2004, Rev. Mod. Phys., 76, 1143
Plotnikov I., Pelletier G., Lemoine M., 2013, MNRAS, 430, 1208
Rabinak I., Katz B., Waxman E., 2011, ApJ, 736, 157
Rossi E., Rees M. J., 2003, MNRAS, 339, 881
Santana R., Barniol-Duran R., Kumar P., 2014, ApJ, 785, 29

Sari R., Esin A. A., 2001, ApJ, 548, 787
Sari R., Piran T., Narayan R., 1998, ApJ, 497, L17
Shaisultanov R., Lyubarsky Y., Eichler D., 2012, ApJ, 744, 182
Sironi L., Spitkovsky A., 2009, ApJ, 698, 1523
Sironi L., Spitkovsky A., 2011, ApJ, 726, 75
Sironi L., Spitkovsky A., Arons J., 2013, ApJ, 771, 54
Spitkovsky A., 2008a, ApJ, 673, L39
Spitkovsky A., 2008b, ApJ, 682, L5
Wang X.-Y., He H.-N., Li Z., Wu X.-F., Dai X.-G., 2010, ApJ, 712, 1232
Wang X.-Y., Liu R., Lemoine M., 2013, ApJ, 771, L33
Wiersma J., Achterberg A., 2004, A&A, 428, 365

This paper has been typeset from a TEX/LATEX file prepared by the author.